Original scientific paper UDK: 539.376:004.942
https://doi.org/10.32762/zr.28.1.2

TRIANGULAR 2D LINKED-INTERPOLATION FINITE ELEMENTS FOR MICROPOLAR CONTINUUM

TROKUTNI 2D MIKROPOLARNI KONAČNI ELEMENTI S VEZANOM INTERPOLACIJOM

Sara Grbčić Erdelj*, Gordan Jelenić*, Dragan Ribarić*

Abstract

Triangular finite elements for linear micropolar continuum theory are developed using linked interpolation. In order to satisfy convergence criteria, the newly presented finite elements are modified using the Petrov-Galerkin method, which uses different interpolation for the test and trial functions. The elements are tested through several numerical examples consisting of a set of patch tests, and a stress concentration problem, and compared to the analytical solution and membrane micropolar finite elements with standard Lagrangian interpolation. All the presented elements faithfully reproduce the micropolar effects in the stress concentration analysis, but the enhancement is negligible with respect to standard Lagrangian elements.

Key words: *micropolar theory, finite element method, linked interpolation, membrane elements*

Sažetak

Razvijena je familija trokutnih konačnih elementa s vezanom interpolacijom kinematičkih polja. Kako bi se zadovoljio kriterij konvergencije konačnog elementa, novi elementi modificirani su Petrov-Galerkinovom aproksimacijom. Elementi su testirani kroz nekoliko numeričkih primjera koji uključuju niz mikropolarnih konvergencijskih testova i problem koncentracije naprezanja. Rezultati su uspoređeni s analitičkim rješenjem i numeričkim rješenjem membranskih mikropolarnih konačnih elemenata sa standardnom Lagrangeovom interpolacijom. Svi predstavljeni elementi vjerno reproduciraju mikropolarne efekte u analizi

* Sveučilište u Rijeci, Građevinski fakultet, Radmile Matejčić 3, 51000 Rijeka
E-mail: {sara.grbcic, gordan.jelenic, dragan.ribaric}@gradri.uniri.hr

Rad zaprimljen: 13.6.2025. Rad prihvaćen: 26.8.2025.

koncentracije naprezanja, iako je poboljšanje zanemarivo u odnosu na standardne Lagrangeove elemente.

Ključne riječi: *mikropolarna teorija, metoda konačnih elemenata, vezana interpolacija, membranski elementi*

1. Introduction

The classical Cauchy continuum theory generally yields accurate predictions for homogeneous materials like steel and aluminium, yet discrepancies arise in cases involving granular, fibrous, or lattice structures. Stress concentrations near holes and notches are often overestimated, and size effects are not captured [1,2]. Moreover, the symmetry constraint on the Cauchy stress tensor restricts the applicability of the classical theory. Further mismatches appear in dynamics, thermal analysis, and fluid flow [1]. To address these limitations, various generalized continuum theories have been proposed [3], among which is the micropolar theory, originating from the Cosserat brothers [4]. In the micropolar theory, in addition to the displacement field, an independent microrotational field is introduced leading to the existence of additional curvature couple-stress tensors. The micropolar material response is governed by six independent constants. Despite its theoretical appeal, practical adoption of the micropolar theory remains limited due to difficulties in determining material parameters. Experimental efforts [2,5] have provided partial insights, but further numerical and experimental developments are essential. The key to improving experimental procedures could lie in numerical analysis of boundary value problems. A comprehensive review of available micropolar finite elements is provided in [3]. In this work, we present triangular finite elements for linear micropolar continuum by using the so-called linked interpolation [6] and assess their performance through several benchmark problems.

2. Micropolar continuum model

2.1 Equilibrium equations

In the state of static equilibrium, we have the following force equilibrium equation

$$\boldsymbol{\sigma}\nabla + \mathbf{p}_{\mathrm{v}} = \mathbf{0}, \tag{1}$$

where ∇ is the differential operator nabla, as well as the moment equilibrium equation

$$\boldsymbol{\mu}\nabla + \mathbf{a} + \mathbf{m}_{\mathrm{v}} = \mathbf{0}, \tag{2}$$

where $\mathbf{a}$ is twice the axial vector of the skew-symmetric part $\boldsymbol{\sigma}_{\mathrm{a}} = \frac{1}{2}\left(\boldsymbol{\sigma} - \boldsymbol{\sigma}^{\mathrm{T}}\right)$ of the stress tensor, i.e.

$$\mathbf{a} = 2\mathrm{axial}(\boldsymbol{\sigma}_{\mathrm{a}}), \tag{3}$$

defined such that $\mathbf{a} \times \mathbf{v} = 2\boldsymbol{\sigma}_{\mathrm{a}}\mathbf{v}$ for any 3D vector $\mathbf{v}$, and $\mathbf{p_v}$, $\mathbf{m_v}$, $\mathbf{p_s}$ and $\mathbf{m_s}$ represent distributed volume and surface force and moment loads, respectively. Attaching a triad of orthogonal base vectors and corresponding Cartesian co-ordinates to the chosen spatial frame of reference, equilibrium equations (1) and (2) may be written as

$$\sigma_{ij,j} + p_{v_i} = 0, \qquad \mu_{ij,j} - \varepsilon_{ijk}\sigma_{jk} + m_{v_i} = 0, \tag{4}$$

where the first index denotes the direction of the stress or axis of the couple stress with respect to the coordinate base, and the second index denotes the direction of the surface normal. The summation convention on repeated indices is implied, and a comma denotes differentiation with respect to a particular spatial coordinate, while ε_{ijk} is the permutation tensor of Levi-Civita. Likewise, the following natural boundary conditions are defined for the part of the body surface subject to applied loading:

$$\boldsymbol{\sigma}\,\mathbf{n} = \mathbf{p}_{\mathrm{s}} \quad \Leftrightarrow \quad \sigma_{ij}n_j = p_{si}, \qquad \boldsymbol{\mu}\,\mathbf{n} = \mathbf{m}_{\mathrm{s}} \quad \Leftrightarrow \quad \mu_{ij}n_j = m_{si}, \tag{5}$$

where $\mathbf{n}$ is the outward unit normal to the surface, along with the essential boundary conditions on the part of the body surface with prescribed kinematics.

2.2 Kinematic equations

In the micropolar continuum theory we have a displacement field $\mathbf{w}(\mathbf{x})$ and an additional kinematic field $\boldsymbol{\varphi}(\mathbf{x})$ known as the microrotation field which represents the local rotation of the point X and is completely independent the macrorotation of the classical continuum theory. The micropolar strain tensor $\boldsymbol{\epsilon}$ is defined as

$$\boldsymbol{\epsilon} = \mathrm{grad}\,\mathbf{w} - \widehat{\boldsymbol{\varphi}} = \mathbf{w} \otimes \nabla - \widehat{\boldsymbol{\varphi}} \quad \Leftrightarrow \quad \epsilon_{ij} = w_{i,j} + \varepsilon_{ijk}\varphi_k, \tag{6}$$

where a superimposed hat on a vector field $(\cdot)$ denotes a skew-symmetric cross-product operator such that $\widehat{(\cdot)}\mathbf{v} = (\cdot) \times \mathbf{v}$ for any 3D vector $\mathbf{v}$. Owing to the existence of an independent rotation field $\boldsymbol{\varphi}$, there also exists a corresponding micropolar curvature tensor

$$\boldsymbol{\kappa} = \mathrm{grad}\,\boldsymbol{\varphi} = \boldsymbol{\varphi} \otimes \nabla \quad \Leftrightarrow \quad \kappa_{ij} = \varphi_{i,j}, \tag{7}$$

where the diagonal terms represent torsional strains. The so-called couple-stress theory is a special case of the micropolar continuum theory, where the microrotation vector $\boldsymbol{\varphi}$ is equal to the macrorotation vector $\boldsymbol{\omega}$ and thus ceases to exist as an independent field.

2.3 Constitutive equations

In a homogeneous isotropic linear elastic micropolar continuum, the stress and couple-stress tensors are related to the strain and curvature tensors, respectively, via constant isotropic fourth-order constitutive tensors, such that in the Cartesian component form we have

$$\sigma_{ij} = \lambda\epsilon_{pp}\delta_{ij} + (\mu + \nu)\epsilon_{ij} + (\mu - \nu)\epsilon_{ji}, \tag{8}$$

$$\mu_{ij} = \alpha\kappa_{pp}\delta_{ij} + (\beta + \gamma)\kappa_{ij} + (\beta - \gamma)\kappa_{ji}, \tag{9}$$

where λ and μ are the Lamé constants, $\nu, \alpha, \beta, \gamma$ are additional material parameters of the linear isotropic micropolar continuum, and δ_{ij} is the Kronecker symbol. The following restrictions on the material parameters hold true as a consequence of positive definiteness of the constitutive tensors: $3\lambda + 2\mu > 0$, $\mu > 0$, $\nu > 0$, $3\alpha + 2\beta > 0$, $\beta > 0$ and $\gamma > 0$. Note that all the stress and strain tensors are now in general non-symmetric. These material parameters may be related to a set of technical (measurable) parameters consisting of shear modulus G, Poisson's ratio n, a dimensionless coupling number between the macrorotation and the microrotation $N \in \langle 0,1 \rangle$, a dimensionless polar ratio of rotation sensitivity (a quantity which relates the torsional strains in a way analogous to that in which Poisson's ratio relates the normal strains) $\psi \in \left\langle 0, \frac{3}{2} \right\rangle$, and the characteristic lengths for torsion and bending l_t and l_b as

$$\begin{gathered} \lambda = \frac{2nG}{1-2n}, \qquad \mu = \mathrm{G}, \qquad \nu = \frac{\mathrm{GN}^2}{1-\mathrm{N}^2}, \\ \alpha = \frac{2\mathrm{Gl}_t^2(1-\psi)}{\psi}, \qquad \beta = \mathrm{Gl}_t^2, \quad \gamma = \mathrm{G}\left(4\mathrm{l}_b^2 - \mathrm{l}_t^2\right). \end{gathered} \tag{10}$$

2.4 Weak form of the equilibrium equations

To construct a numerical solution procedure of the boundary value problem analysed, we state that the virtual work of external forces must be equal to the virtual work of the internal forces

$$G^{int}(\mathbf{w}, \boldsymbol{\varphi}; \overline{\mathbf{w}}, \overline{\boldsymbol{\varphi}}) = G^{ext}(\overline{\mathbf{w}}, \overline{\boldsymbol{\varphi}}), \tag{11}$$

with the virtual works of internal and external forces defined as

$$G^{int}(\mathbf{w}, \boldsymbol{\varphi}; \overline{\mathbf{w}}, \overline{\boldsymbol{\varphi}}) = \int_V (\overline{\boldsymbol{\epsilon}} : \boldsymbol{\sigma} + \overline{\boldsymbol{\kappa}} : \boldsymbol{\mu}) dV, \tag{12}$$

$$G^{int}(\overline{\mathbf{w}}, \overline{\boldsymbol{\varphi}}) = \int_V (\overline{\mathbf{w}} \cdot \mathbf{p}_\mathrm{v} + \overline{\boldsymbol{\varphi}} \cdot \mathbf{m}_\mathrm{v})\, dV - \int_S (\overline{\mathbf{w}} \cdot \mathbf{p}_\mathrm{s} + \overline{\boldsymbol{\varphi}} \cdot \mathbf{m}_\mathrm{s})\, dS, \tag{13}$$

where $\overline{\mathbf{w}}$ and $\overline{\boldsymbol{\varphi}}$ are the virtual displacement and microrotation vectors and $\overline{\boldsymbol{\epsilon}}$ and $\overline{\boldsymbol{\kappa}}$ are the corresponding tensors of virtual micropolar strains

and curvatures, respectively. The algebraic equilibrium equations of the finite element method will be thus obtained after an appropriate interpolation of the kinematic fields and their virtual counterparts has been specified. In the following section, we propose a generalisation of the standard Lagrangian interpolation, which includes the rotational degrees of freedom in the interpolation of the displacement vector - the so-called linked interpolation.

3. Governing equations of a 2D micropolar continuum

In order to develop membrane finite elements, the presented boundary value problem is reduced from 3D to 2D. Consequently, the kinematic fields are in Cartesian coordinates reduced to only two independent displacements $\mathbf{w} = \langle u\ v\ 0 \rangle^{\mathrm{T}}$ and one microrotation $\boldsymbol{\varphi} = \langle 0\ 0\ \varphi \rangle^{\mathrm{T}}$, which represents an in-plane (or drilling) rotation. Furthermore, assuming a plane-strain condition, the stress and strain tensors are reduced to $\boldsymbol{\sigma} = \langle \sigma_{11}\ \sigma_{12}\ \sigma_{21}\ \sigma_{22} \rangle^{\mathrm{T}}$, $\boldsymbol{\mu} = \langle \mu_{31}\ \mu_{32} \rangle^{\mathrm{T}}$ and $\boldsymbol{\epsilon} = \langle \epsilon_{11}\ \epsilon_{12}\ \epsilon_{21}\ \epsilon_{22} \rangle^{\mathrm{T}}$, $\boldsymbol{\kappa} = \langle \kappa_{31}\ \kappa_{32} \rangle^{\mathrm{T}}$ respectively with

$$\begin{Bmatrix} \sigma_{11} \\ \sigma_{12} \\ \sigma_{21} \\ \sigma_{22} \end{Bmatrix} = \begin{bmatrix} (\lambda + 2\mu) & 0 & 0 & \lambda \\ 0 & (\mu + \nu) & (\mu - \nu) & 0 \\ 0 & (\mu - \nu) & (\mu + \nu) & 0 \\ \lambda & 0 & 0 & (\lambda + 2\mu) \end{bmatrix} \begin{Bmatrix} \epsilon_{11} \\ \epsilon_{12} \\ \epsilon_{21} \\ \epsilon_{22} \end{Bmatrix} \quad \Leftrightarrow \quad \boldsymbol{\sigma} = \mathbf{C_1}\boldsymbol{\epsilon},$$

$$\begin{Bmatrix} \mu_{31} \\ \mu_{32} \end{Bmatrix} = \begin{bmatrix} (\beta + \gamma) & 0 \\ 0 & (\beta + \gamma) \end{bmatrix} \begin{Bmatrix} \kappa_{31} \\ \kappa_{32} \end{Bmatrix} \quad \Leftrightarrow \quad \boldsymbol{\mu} = \mathbf{C_2}\boldsymbol{\kappa}, \tag{14}$$

where $\mathbf{C_1}$ and $\mathbf{C_2}$ stand for the micropolar constitutive tensors. Therefore, the problem is reduced to only four elastic constants λ, μ, ν, and $\beta + \gamma$. The applied loading is likewise reduced to

$$\mathbf{p}_{\mathrm{v}} = \begin{Bmatrix} p_{v1} \\ p_{v2} \\ 0 \end{Bmatrix} = \begin{Bmatrix} \mathbf{q}_{\mathrm{v}} \\ 0 \end{Bmatrix}, \ \mathbf{m}_{\mathrm{v}} = \begin{Bmatrix} 0 \\ 0 \\ m_v \end{Bmatrix}, \tag{15}$$

$$\mathbf{p}_{\mathrm{s}} = \begin{Bmatrix} p_{s1} \\ p_{s2} \\ 0 \end{Bmatrix} = \begin{Bmatrix} \mathbf{q}_{\mathrm{s}} \\ 0 \end{Bmatrix}, \ \mathbf{m}_{\mathrm{s}} = \begin{Bmatrix} 0 \\ 0 \\ m_s \end{Bmatrix}. \tag{16}$$

The kinematic equations are reduced to

$$\begin{Bmatrix}\epsilon_{11}\\ \epsilon_{12}\\ \epsilon_{21}\\ \epsilon_{22}\end{Bmatrix}=\begin{bmatrix}\dfrac{\partial}{\partial x} & 0\\ \dfrac{\partial}{\partial y} & 0\\ 0 & \dfrac{\partial}{\partial x}\\ 0 & \dfrac{\partial}{\partial y}\end{bmatrix}\begin{Bmatrix}u\\ v\end{Bmatrix}+\varphi\begin{Bmatrix}0\\ 1\\ -1\\ 0\end{Bmatrix}\quad\Leftrightarrow\quad \boldsymbol{\epsilon}=\mathbf{D_u}^{\mathrm{T}}\mathbf{u}+\varphi\mathbf{I}_{\varphi}, \tag{17}$$

while the curvatures are reduced to

$$\begin{Bmatrix}\kappa_{31}\\ \kappa_{32}\end{Bmatrix}=\begin{Bmatrix}\dfrac{\partial}{\partial x}\\ \dfrac{\partial}{\partial y}\end{Bmatrix}\varphi=\mathbf{D_\mu}^{\mathrm{T}}\varphi. \tag{18}$$

In order to obtain the numerical solution of the problem, the kinematic fields have to be approximated using a chosen type of interpolation. In general, the real and virtual kinematic fields are interpolated as $\mathbf{u}^h=\mathbf{N_u}\,\mathbf{d}^e$, $\varphi^h=\mathbf{N_\varphi}\,\mathbf{d}^e$, $\overline{\mathbf{u}}^h=\mathbf{N_u}\,\overline{\mathbf{d}}^e$, $\overline{\varphi}^h=\mathbf{N_\varphi}\,\overline{\mathbf{d}}^e$, where $\mathbf{N_u}$ and $\mathbf{N_\varphi}$ represent the matrices of interpolation functions over an element for the displacement and microrotation field, respectively, and $\mathbf{d}^e$ and $\overline{\mathbf{d}}^e$ represent the real and virtual vector of element nodal degrees of freedom, respectively. Superscript h denotes the discretization, while e denotes the element to which the interpolation is applied. After introducing the interpolation and substituting the kinematic and constitutive equations we obtain the interpolated element internal and external virtual works as

$$\begin{aligned}G^{int,e}\left(\mathbf{d}^e;\overline{\mathbf{d}}^e\right)=\;&\overline{\mathbf{d}}^{e\mathrm{T}}\int_V\left(\mathbf{N_u}^{\mathrm{T}}\mathbf{D_u}+\mathbf{N_\varphi}^{\mathrm{T}}\mathbf{I_\varphi}^{\mathrm{T}}\right)\mathbf{C_1}\left(\mathbf{D_u}^{\mathrm{T}}\mathbf{N_u}+\mathbf{I_\varphi}\mathbf{N_\varphi}\right)dV\,\mathbf{d}^e+\\ &\overline{\mathbf{d}}^{e\mathrm{T}}\int_V\left(\mathbf{N_\varphi}^{\mathrm{T}}\mathbf{D_\varphi}\right)\mathbf{C_2}\left(\mathbf{D_\varphi}^{\mathrm{T}}\mathbf{N_\varphi}\right)dV\,\mathbf{d}^e=\overline{\mathbf{d}}^{e\mathrm{T}}\mathbf{K}^e\mathbf{d}^e,\end{aligned} \tag{19}$$

$$\begin{aligned}G^{ext,e}\left(\overline{\mathbf{d}}^e\right)=\;&\overline{\mathbf{d}}^{e\mathrm{T}}\int_V\left(\mathbf{N_u}^{\mathrm{T}}\mathbf{q}_{\mathrm{v}}+\mathbf{N_\varphi}^{\mathrm{T}}\mathbf{m}_{\mathrm{v}}\right)dV+\overline{\mathbf{d}}^{e\mathrm{T}}\int_S\left(\mathbf{N_u}^{\mathrm{T}}\mathbf{q}_{\mathrm{s}}+\mathbf{N_\varphi}^{\mathrm{T}}\mathbf{m}_{\mathrm{s}}\right)dS\\ =\;&\overline{\mathbf{d}}^{e\mathrm{T}}\mathbf{f}^e,\end{aligned}$$

where $\mathbf{K}^e$ and $\mathbf{f}^e$ represent the element stiffness matrix and external force vector. The global internal and external virtual works are obtained as

$$\begin{aligned}G^{int}(\mathbf{d};\overline{\mathbf{d}})=&\mathop{\mathbb{A}}_{e=1}^{n_{elem}}G^{int,e}\left(\mathbf{d}^e;\overline{\mathbf{d}}^e\right)\equiv\overline{\mathbf{d}}^{\mathrm{T}}\mathbf{K}\mathbf{d},\quad G^{ext}(\overline{\mathbf{d}})=\mathop{\mathbb{A}}_{e=1}^{n_{elem}}G^{ext,e}\left(\overline{\mathbf{d}}^e\right)\\ &\equiv\overline{\mathbf{d}}^{\mathrm{T}}\mathbf{f}\end{aligned}$$

with $\mathbf{d}$ and $\overline{\mathbf{d}}$ as the global vectors of real and virtual displacements, $\mathbf{K}=\mathop{\mathbb{A}}_{e=1}^{n_{elem}}\mathbf{K}^e$ and $\mathbf{f}=\mathop{\mathbb{A}}_{e=1}^{n_{elem}}\mathbf{f}^e$ as the global stiffness matrix and external

force vector, n_{elem} as the total number of elements in the mesh, and $\mathbb{A}$ as the finite-element assembly operator. Finally, substituting G^{int} and G^{ext} we obtain the approximated weak form. Recognising arbitrariness of $\overline{\mathbf{d}}$, we eventually obtain the basic set of algebraic equations of the finite element method as $\mathbf{K}\,\mathbf{d} = \mathbf{f}$.

4. Lagrangian and linked interpolation

In this paper two different interpolations are compared for the family of triangular finite elements. The first one is the conventional Lagrange interpolation, serving to approximate the real and virtual displacements as

$$\mathbf{u}^h = \mathbf{N}_u \mathbf{d}^e, \quad \overline{\mathbf{u}}^h = \mathbf{N}_u \overline{\mathbf{d}}^e, \tag{20}$$

and the real and virtual microrotation as

$$\varphi^h = \mathbf{N}_{\boldsymbol{\varphi}}\, \mathbf{d}^e, \quad \overline{\varphi}^h = \mathbf{N}_{\boldsymbol{\varphi}}\, \overline{\mathbf{d}}^e, \tag{21}$$

with

$$\mathbf{N}_u = \begin{bmatrix} N_1 & 0 & 0 & \dots & N_{n_{node}} & 0 & 0 \\ 0 & N_1 & 0 & \dots & 0 & N_{n_{node}} & 0 \end{bmatrix} \quad \text{and}$$

$$\mathbf{N}_{\boldsymbol{\varphi}} = \langle 0 \quad 0 \quad N_1 \quad \dots \quad 0 \quad 0 \quad N_{n_{node}} \rangle,$$

n_{node} as the number of nodes on the element and $N_i (i = 1, \dots, n_{node})$ as the i^{th} Lagrangian polynomial. The second interpolation analysed is the linked interpolation in which the displacement field depends on the nodal microrotation, too. The linked interpolation for the displacement field consists of the conventional Lagrange interpolation (represented by matrix $\mathbf{N}_u$) enhanced by the contribution due to the nodal microrotations. In general, the linked interpolation is therefore given as

$$\mathbf{u}^h = (\mathbf{N}_u + \mathbf{N}_{enh})\mathbf{d}^e, \quad \overline{\mathbf{u}}^h = (\mathbf{N}_u + \mathbf{N}_{enh})\overline{\mathbf{d}}^e, \tag{22}$$

where $\mathbf{N}_{enh}$ is the matrix of linked-interpolation enhancement to the Lagrangian interpolation. In the linked-interpolation framework, the microrotations are still interpolated conventionally, as defined in equation (21). The linked interpolation is in [6] derived as the exact solution of differential equations of a 3D Timoshenko beam. For the present purposes let us limit our attention to its 2D form, where the displacement field along the in-plane axis z orthogonal to the centroidal line x of the beam is

$$w = \sum_{i=1}^{n_{node}} N_i\, w_i - \frac{L}{n_{node}} \sum_{i=1}^{n_{node}} \frac{\xi - \xi_i}{2} N_i \varphi_i, \tag{23}$$

while the rotation field around the out-of-plane axis y orthogonal to the centroidal line is simply

$$\varphi = \sum_{i=1}^{n_{node}} N_i \, \varphi_i, \tag{24}$$

where L is the finite-element length, $\xi \in [-1,1]$ is the natural co-ordinate, n_{node} is the number of nodes on the element, φ_i and w_i are the rotation and the displacement at the i^{th} node, N_i is the i^{th} Lagrange polynomial of order $n_{node} - 1$, ξ_i is the natural co-ordinate of the i^{th} node, and the axes x, y, z form a right-handed co-ordinate system. The displacement field is thus interpolated by a polynomial, one order higher than that used for the rotations. The Lagrangian polynomials are given as

$$N_i = \prod_{\substack{j=1 \\ j \neq i}}^{n_{node}} \frac{(\xi_j - \xi)}{(\xi_j - \xi_i)}, \quad i = 1, \ldots, n_{node}. \tag{25}$$

In order to generalise the linked interpolation concept presented to 2D micropolar continuum, it is important to note that, in contrast to beams, a closed-form solution of the differential equations does not generally exist for this continuum. The approach that we take is the following: (i) we apply interpolation (23) to the element edges only, i.e. we treat the element edges as beam finite elements and (ii) we average the edge results within the interior of the element depending on the actual position so that that interpolation correctly describes rigid-body motion. To do this, we follow the approach proposed in [7] for the Mindlin plate elements.

4.1 Triangular finite elements

The triangular finite element family with the related shape functions is defined in the natural coordinate system. The mapping from the natural coordinate system (ξ, η) to the Cartesian coordinate system (x, y) is defined as:

$$x = \sum_{a=1}^{n_{node}} N_a \, (\xi, \eta) x_a, \quad y = \sum_{a=1}^{n_{node}} N_a \, (\xi, \eta) y_a, \tag{26}$$

where n_{node} stands for the number of element nodes, (x_a, y_a) represent the element nodal coordinates in the Cartesian coordinate system and $N_a(\xi, \eta)$ represent the isoparametric shape functions with arguments ξ, η, which run between [0,1]. Here we consider the elements with three, six or ten nodes, with a node-numbering convention as shown in Figure 1.

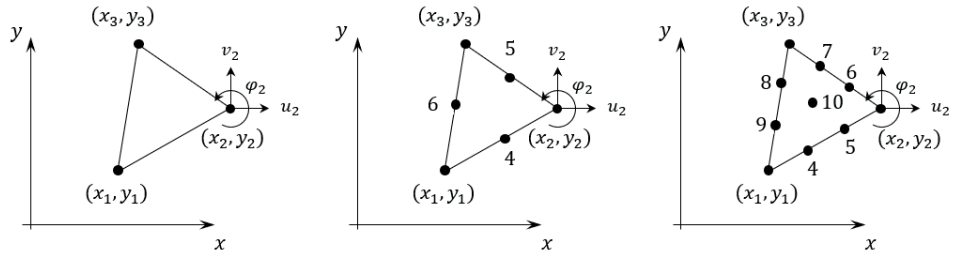

(a) T3 (b) T6 (c) T10

Figure 1. Triangular finite elements of different order

The shape functions are most easily expressed via a set of the so-called area coordinates

$$\zeta_1(\xi,\eta) = 1 - \xi - \eta, \quad \zeta_2(\xi,\eta) = \xi, \quad \zeta_3(\xi,\eta) = \eta. \tag{27}$$

The triangular shape functions for the edge nodes in Figure 1 taken at the edge halves in T6 and at the edge thirds in T10 and the inner node in T10 in its centroid are given in Table 1. For the Lagrangian family of elements, the same shape functions are used for the interpolation of real and virtual displacements and rotations as given in equations (20) and (21). For the family of elements with linked interpolation, the rotations are still interpolated using the Lagrange polynomials and (21), but in the displacement field we now have an enhancement in the displacement field as shown in equation (22). For the elements of different order, this enhancement is now defined following the approach given in [7].

Table 1. *Triangular shape functions*

Element	T3	T6	T10
Vertex:	$N_a = \zeta_a$	$N_a = \zeta_a(2\zeta_a - 1)$	$N_a = \frac{1}{2}\zeta_a(3\zeta_a - 1)(3\zeta_a - 2)$
Edge:	-	$N_{i+3} = 4\zeta_i\zeta_j$	$N_{2i+2} = \frac{9}{2}\zeta_i\zeta_j(3\zeta_i - 1)$ $N_{2i+3} = \frac{9}{2}\zeta_i\zeta_j(3\zeta_j - 1)$
Centroid node:	-	-	$N_{10} = 27\zeta_1\zeta_2\zeta_3$

4.1.1 Triangular membrane element with three nodes (T3LI)

In analogy with the linked interpolation for a beam element (23), when applied to a two-noded beam, we propose the linked interpolation for the triangular element with three nodes and three degrees of freedom per node, named T3LI and shown in Figure 1, such that

$$\begin{aligned}\mathbf{u}^h &= (\mathbf{N}_u + \mathbf{N}_{enh})\mathbf{d}^e \\ &= \sum_{a=1}^{3} N_a\,\mathbf{u}_a + \frac{1}{2}\zeta_2\zeta_3(\varphi_2-\varphi_3)\begin{Bmatrix} y_2-y_3 \\ x_3-x_2\end{Bmatrix} + \frac{1}{2}\zeta_3\zeta_1(\varphi_3-\varphi_1)\begin{Bmatrix} y_3-y_1 \\ x_1-x_3\end{Bmatrix} + \\ &\quad + \frac{1}{2}\zeta_1\zeta_2(\varphi_1-\varphi_2)\begin{Bmatrix} y_1-y_2 \\ x_2-x_1\end{Bmatrix} \\ &= \sum_{a=1}^{3} N_a\,\mathbf{u}_a + \begin{Bmatrix} f_{1,x} \\ f_{1,y}\end{Bmatrix}(\varphi_2-\varphi_3) + \begin{Bmatrix} f_{2,x} \\ f_{2,y}\end{Bmatrix}(\varphi_3-\varphi_1) + \begin{Bmatrix} f_{3,x} \\ f_{3,y}\end{Bmatrix}(\varphi_1-\varphi_2)\end{aligned} \tag{28}$$

where $f_{i,x} = \frac{1}{2}\zeta_j\zeta_k(y_j - y_k)$, $f_{i,y} = \frac{1}{2}\zeta_j\zeta_k(x_k - x_j)$ and i, j, k is a cyclic permutation of 1,2,3 resulting in $\mathbf{N}_{enh} = [\mathbf{N}_{enh,1} \quad \mathbf{N}_{enh,2} \quad \mathbf{N}_{enh,3}]$, where

$$\mathbf{N}_{enh,i} = \begin{bmatrix} 0 & 0 & f_{k,x} - f_{j,x} \\ 0 & 0 & f_{k,y} - f_{j,y}\end{bmatrix}. \tag{29}$$

4.1.2 Triangular membrane element with six nodes (T6LI)

Now we generalise the linked interpolation of a beam element applied to a three-noded beam to a triangular element with six nodes and three degrees of freedom per node, named T6LI. The displacement interpolation thus follows as

$$\begin{aligned}\mathbf{u}^h = (\mathbf{N}_u + \mathbf{N}_{enh})\mathbf{d}^e \quad &= \sum_{a=1}^{6} N_a(\xi,\eta)\begin{Bmatrix} u_a \\ v_a\end{Bmatrix} + \\ &+ \frac{1}{3}\zeta_1\zeta_2(\zeta_2-\zeta_1)(\varphi_1 - 2\varphi_4 + \varphi_2)\begin{Bmatrix} y_2-y_1 \\ x_1-x_2\end{Bmatrix} + \\ &+ \frac{1}{3}\zeta_2\zeta_3(\zeta_3-\zeta_2)(\varphi_2 - 2\varphi_5 + \varphi_3)\begin{Bmatrix} y_3-y_2 \\ x_2-x_3\end{Bmatrix} + \\ &+ \frac{1}{3}\zeta_3\zeta_1(\zeta_1-\zeta_3)(\varphi_3 - 2\varphi_6 + \varphi_1)\begin{Bmatrix} y_1-y_3 \\ x_3-x_1\end{Bmatrix}\end{aligned} \tag{30}$$

from where $\mathbf{N}_{enh}$ immediately follows.

4.1.3 Triangular membrane element with ten nodes (T10LI)

Finally, we develop the triangular element with ten nodes shown in Figure 1., which we name T10LI. Generalising the linked interpolation for a beam element applied to a four-node element

$$\begin{aligned}\mathbf{u}^h = \quad & (\mathbf{N}_u + \mathbf{N}_{enh})\mathbf{d}^e = \sum_{a=1}^{10} N_a(\xi,\eta)\begin{Bmatrix} u_a \\ v_a \end{Bmatrix} + \\ & + \frac{1}{8}\zeta_1\zeta_2(3\zeta_1 - 1)(3\zeta_2 - 1)\begin{Bmatrix} y_2 - y_1 \\ x_1 - x_2 \end{Bmatrix}(\varphi_1 - 3\varphi_4 + 3\varphi_5 - \varphi_2) + \\ & + \frac{1}{8}\zeta_2\zeta_3(3\zeta_2 - 1)(3\zeta_3 - 1)\begin{Bmatrix} y_3 - y_2 \\ x_2 - x_3 \end{Bmatrix}(\varphi_2 - 3\varphi_6 + 3\varphi_7 - \varphi_3) + \\ & + \frac{1}{8}\zeta_3\zeta_1(3\zeta_3 - 1)(3\zeta_1 - 1)\begin{Bmatrix} y_1 - y_3 \\ x_3 - x_1 \end{Bmatrix}(\varphi_3 - 3\varphi_8 + 3\varphi_9 - \varphi_1),\end{aligned} \tag{31}$$

from where $\mathbf{N}_{enh}$ again immediately follows.

5. Numerical examples

In this section the presented family of triangular elements is analysed through several numerical examples. The convergence analysis is performed on a force patch test using a regular mesh, and the conclusions drawn are implemented in the procedure to run the displacement patch test on an irregular mesh. Next, an infinite plate with a cylindrical hole subject to uniform tension is analysed and the results are compared to the analytical solution. In all the examples, both the standard Lagrange finite elements and the newly presented linked-interpolation finite elements are tested.

5.1 Force patch test: cantilever beam subject to pure tension

A force patch test is performed on a cantilever beam of length $L = 10$ m, height $h = 2$ m and a unit thickness subject to pure axial distributed loading $p = 10\ \mathrm{N/m^2}$ using a number of regular meshes. The micropolar material parameters used are equal to $\mu = 1000\ \mathrm{N/m^2}$, $\lambda = 1000\ \mathrm{N/m^2}$, $\nu = 500\ \mathrm{N/m^2}$ and $\beta = \gamma = 20$ N. In this example, the analytical results for the stress fields and the axial displacement at the free end (pL/E) are expected to be obtained for an arbitrary number of finite elements in the mesh. The triangular finite elements with the conventional (Lagrange) interpolation passed the test, while the first and third order elements with the newly proposed linked interpolation failed. To understand why two of the linked-interpolation elements fail this test and find the solution for how to modify them in order to pass it, an inversely posed problem has been studied: the correct nodal displacement and rotations have been prescribed to the elements with linked interpolation and the resulting stress and couple-stress tensors as well as the nodal load vector have been analysed. It turns out that the all the stress and stress-couple components are exact but, in the nodal load vector, the incorrect moment components are generated by the linked interpolation applied to

the virtual displacements. Interestingly, this does not happen in the quadratic element T6+LI. Motivated by this observation, a solution is found by applying the *Petrov–Galerkin* finite-element method, which is based on *different interpolation* for the test and the trail functions – here the virtual and the actual displacement fields. To eliminate the anomalous nodal moments caused by the linked interpolation of the virtual displacements $\overline{\mathbf{u}}$, here we choose to *interpolate them using the standard Lagrangian polynomials*, i.e.

$$\overline{\mathbf{u}} = \mathbf{N}_u \overline{\mathbf{d}}, \tag{32}$$

The real displacements, however, are still interpolated using the linked interpolation, i.e.

$$\mathbf{u} = (\mathbf{N}_u + \mathbf{N}_{enh})\mathbf{d}, \tag{33}$$

The microrotation interpolation remains unchanged in both its virtual and its real form, i.e. $\overline{\varphi} = \mathbf{N}_\varphi \overline{\mathbf{d}}$ and $\varphi = \mathbf{N}_\varphi \mathbf{d}$. The Petrov-Galerkin modification described is applied to those elements which fail the patch test. We refer to these elements as T3LIPG, T10LIPG. When performing the same patch test using the elements based on the Petrov-Galerkin method, the patch test for all the elements is passed. To understand why the quadratic elements with linked interpolation (T6LI) pass this patch test, while the linear and the cubic elements (T3LI and T10LI) do not, let us pinpoint the main difference between these two groups of elements in the character of the enhanced shape functions caused by the linked interpolation. In the linear and the cubic elements, the enhancement is symmetric, which, when integrated over the element domain, gives a non-zero value, and thus provides non-desired nodal moments for the constant-stress state present here. On the other hand, the enhanced interpolation functions for the quadratic elements are antisymmetric and thus integrate to zero for the constant-stress state. In the work of Grbac et al. [9], this problem is solved by interpolating the external body and surface loads in accordance with the chosen interpolation, as defined in equation, for hexahedral elements, which results in additional nodal moment forces. As a result, the first order hexahedral finite element provides the analytical solution without the need to use the Petrov-Galerking method.

5.2 Displacement patch tests for the micropolar continuum

According to Providas [10], the patch test for micropolar finite elements should consist of a set of three separate tests. The tests are performed on a rectangular domain bounded by the sides connecting the points 1–4 and discretised using the distorted finite-element mesh shown. The length and height of the domain are $L = 0.24$ m, $H = 0.12$ m and the coordinates of the internal nodes 5–8 are the following 5=(0.04,0.02),

6=(0.18,0.03), 7=(0.08,0.08) and 8=(0.16,0.08). The material parameters used are the same as defined in the force patch test example. The displacements and microrotations are imposed on the external nodes, while the volume loading (if any) is imposed on the interior of the domain. The element passes a patch test if the internal nodes are capable of reproducing the analytical solution imposed by the boundary conditions.

The first test is the standard patch test of the finite elements in the classical continuum theory, whereby imposing linearly varying displacement and a constant microrotation field via appropriate boundary conditions we obtain the state of constant symmetric stress and strain. The fields are defined as $u = 10^{-3}(x + 0.5y)$, $v = 10^{-3}(x + y)$, $\varphi = 0.25 \cdot 10^{-3}$.

The second test describes the state of constant non-symmetric shear, for which a constant body moment is needed. The actual input is given as $u = 10^{-3}(x + 0.5y)$, $v = 10^{-3}(x + y)$, $\varphi = 0.75 \cdot 10^{-3}$, $m_v = 1$.

The third test describes the state of constant curvature, whereby imposing linearly varying displacement, microrotation and body moment fields as well as a constant body force field we obtain linearly varying stresses and constant couple-stresses. Providas [10] considers the third patch test to be a necessary condition for finite-element convergence even though in this test the shear stresses are linearly varying, i.e. $u = 10^{-3}(x + 0.5y)$, $v = 10^{-3}(x + y)$, $\varphi = 10^{-3}\,(0.25 + (x - y))$, $p_x = p_y = 1$, $m_v = 2(x - y)$. However, satisfaction of a patch test in which stress distribution is variable is not necessary for convergence and, for this reason, we consider this test to be a higher-order patch test, analogous to a pure bending test.

All the proposed elements pass the constant stress tests. Regarding the third test, all the elements in which the standard Lagrangian interpolation has been utilised pass, which is expected even though it contradicts the results in the literature. For the highest-order element T10, however, the amount of data provided on the boundary has not been sufficient and four additional internal nodes have had to be additionally prescribed the field values to pass it. Concerning the family of elements with linked interpolation, T3LIPG fail to pass this test, while all the higher-order elements pass it. The results of the third test for the elements, which do not pass it, are presented in Table 2. Even though this patch test is not satisfied for the lower-order element of finite size, we consider that all the proposed elements satisfy the convergence criteria since, as argued earlier, they are able to reproduce exactly any state of constant stress.

***Table 2**. Results for Patch test 3*

Element	$u * 10^{-3}$	$v * 10^{-3}$	$\varphi * 10^{-3}$	σ_{11}	σ_{12}	σ_{21}	μ_{31}	μ_{32}
T3	0.195	0.210	0.400	4.00	1.59	1.41	0.04	-0.04
T3LIPG	0.194	0.205	0.401	4.01	1.54	1.36	0.04	-0.04
Exact	0.195	0.210	0.400	4.00	1.59	1.41	0.04	-0.04

5.3 Stress concentration around a circular hole

To analyse the influence of the micropolar effect in a homogeneous and isotropic linear elastic solid, the so-called Kirsch problem, an infinite plate with a circular hole subject to uniform tension is considered next. We focus on the so-called *stress-concentration factor (K_t)* – the ratio between a maximum longitudinal stress at the edge of the hole and the applied surface loading. The classical theory predicts a constant stress concentration factor equal to three regardless of the hole size and the material parameters. Experimental tests indicate a smaller stress-concentration factor than that. The analytical solution of the problem using the micropolar theory [11] is dependent on the hole radius r, the coupling number N and the characteristic length l of the material and it returns the stress-concentration factor which is increasingly smaller than the one obtained by the classical theory as the diameter of the hole decreases.
In our numerical analysis, the plate is necessarily taken to be of a finite size and only a quarter of the plate is analysed. The square quarter is taken to be of unit thickness, $L = 16.2$ mm long and with a hole of radius $r = 0.216$ mm subject to uniform uniaxial tension $p = 1$ N/mm^2 acting on one of its undented sides. The micropolar material parameters $\mu = 76923.1$ N/mm^2, $\lambda = 115385.0$ N/mm^2, $\beta = \gamma = 6352.25$ N, which correspond to the modulus of elasticity $E = 200000$ N/mm^2, Poisson's ratio $n = 0.3$ and a characteristic length $l = r/1.063 = 0.2031984948$ m are taken from [10]. The value of the micropolar material parameter ν is varied (indicating a variation in the coupling number N). The normal displacements and the microrotations along the dented sides are restrained. The results obtained by the proposed triangular finite elements with linked interpolation are compared to those obtained by the finite elements with standard Lagrangian interpolation. The finite element mesh, shown in Figure 2, consist of 360 elements. In the structured part of the mesh the finite elements project radially from the hole and are embedded within 22 concentric circles propagating in geometric progression with ratio between the radial increments of 1.2. The part of the mesh between the outermost band of the elements between the concentric circles and the undented edges is defined manually. The stresses are observed in the element containing the stress-concentration point P=(0.0, 0.216), where

the analytical solution is provided. To avoid extrapolation of the computed stresses, the stress values for the numerical simulation are given at Gauss points closest to the edge of the hole, not at the exact edge, thus they can never exactly match the analytical result. The Gauss points monitored have the co-ordinates equal to GP1=(0.0025, 0.2435), GP2=(0.0199, 0.2184) and GP3=(0.0199, 0.2184). The results for the stresses obtained are shown in Table 2. The numerical results for all the elements show that with the micropolar effect increased the stress-concentration factor is reduced, as predicted theoretically. The predictive power of all the elements, however, decreases as the coupling number increases. With the higher-order elements, the linked-interpolation elements' behaviour is exceedingly close to that of the standard elements, i.e. these elements do not contribute to the faster convergence rate. Interestingly, the higher-order linked-interpolation element T6LI does behave marginally better than its Lagrangian counterparts when there is no micropolar effect present. With the low-order triangular elements, the linked-interpolation slightly improves the accuracy, this time, however, with an increasing micropolar effect. This behaviour is not observed in the low-order quadrilateral elements [8].

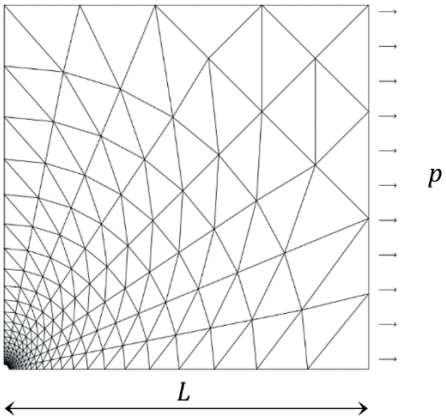

Figure 2. Triangular finite-element mesh for the Kirsch problem

***Table 2**. Stress-concentration factor K_t*

N	K_t	EL	K_t, GP1	EL	K_t, GP2	EL	K_t, GP3
0.00	3.000	T3	2.846	T6	2.865	T10	2.849
		T3LIPG	2.846	T6LI	2.897	T10LIPG	2.849
0.25	2.849	T3	2.737	T6	2.729	T10	2.715
		T3LIPG	2.740	T6LI	2.729	T10LIPG	2.715
0.50	2.555	T3	2.508	T6	2.466	T10	2.454
		T3LIPG	2.514	T6LI	2.466	T10LIPG	2.454
0.75	2.287	T3	2.267	T6	2.228	T10	2.219
		T3LIPG	2.273	T6LI	2.228	T10LIPG	2.219
0.9	2.158	T3	2.101	T6	2.117	T10	2.108
		T3LIPG	2.109	T6LI	2.117	T10LIPG	2.108

6. Conclusion

A new family of membrane finite elements interpolated using the linked-interpolation concept for the analysis of the micropolar continuum theory is presented. Triangular elements of different order are developed and tested through four numerical examples and compared to the conventional elements interpolated using the Lagrangian interpolation. In order to assure convergence, the proposed linked-interpolation finite elements are modified using Petrov-Galerkin interpolation. For the infinite plate with circular hole benchmark problem, the newly proposed finite elements correctly reproduce the amount of stress concentration predicted by the micropolar theory, but they are only marginally more accurate than their Lagrangian counterparts.

Literatura

[1] Nowacki, W. (1972). Theory of Micropolar Elasticity. Vienna: Springer-Verlag.

[2] Lakes, R. S. (1983). Size Effects and Micromechanics of a Porous Solid. Journal of Materials Science, 18, 2572–2580.

[3] Eringen, A. C. (2012). Microcontinuum Field Theories: I. Foundations and Solids. New York: Springer-Verlag.

[4] Cosserat, E., Cosserat, F. (1909). Théorie des corps déformables. Paris: Herman.

[5] Gauthier, R., Jahsman, W. E. (1975). A Quest for Micropolar Elastic Constants. Journal of Applied Mechanics, 42(2), 369–374.

[6] Jelenić, G., Papa, E. (2011). Exact Solution of 3D Timoshenko Beam Problem Using Linked Interpolation of Arbitrary Order. Archive of Applied Mechanics, 81(2), 171–183.

[7] Ribarić, D., Jelenić, G. (2014). Higher-Order Linked Interpolation in Triangular Thick Plate Finite Elements. Engineering Computations, 31(1), 69–109.

[8] Grbčić, S., Jelenić, G., Ribarić, D. (2019). Quadrilateral 2D Linked-Interpolation Finite Elements for Micropolar Continuum. Acta Mechanica Sinic, 35, 1001–1020.

[9] Grbac, L., Jelenić, G., Ribarić, D., Grbčić Erdelj, S. (2024). Hexahedral Finite Elements with Enhanced Fixed-Pole Interpolation for Linear Static and Vibration Analysis of 3D Micropolar Continuum. International Journal for Numerical Methods in Engineering, 125(8), e7440.

[10] Providas, E., Kattis, M.A. (2002). Finite Element Method in Plane Cosserat Elasticity, Computers and Structures, 80, 2059-2069.

[11] Kirsch, E. (1898). Die Theorie der Elastizität und die Bedürfnisse der Festigkeitslehre. Zeitschrift des Vereines deutscher Ingenieure, 42, 797–807.